Hindawi
International Journal of Antennas and Propagation
Volume 2019, Article ID 2463871, 11 pages
https://doi.org/10.1155/2019/2463871

Research Article

Circularly Polarized Omnidirectional Antenna with Dipole Core and Diagonally Adjoined Parasitic Braces for ISM Band Applications

Piyapong Dangkham[1], **Sitthichai Dentri**[2], **Chuwong Phongcharoenpanich**[1] and **Prayoot Akkaraekthalin**[3]

[1]*Faculty of Engineering, King Mongkut's Institute of Technology Ladkrabang, Bangkok, Thailand*
[2]*Department of Electronics Engineering Technology, College of Industrial Technology, King Mongkut's University of Technology North Bangkok, Bangkok, Thailand*
[3]*Department of Electrical and Computer Engineering, Faculty of Engineering, King Mongkut's University of Technology North Bangkok, Bangkok, Thailand*

Correspondence should be addressed to Sitthichai Dentri; sitthichaid@kmutnb.ac.th

Received 1 February 2019; Revised 13 April 2019; Accepted 16 May 2019; Published 21 August 2019

Academic Editor: Xianming Qing

This research proposes a circularly polarized (CP) single-fed omnidirectional dipole antenna operable in 2.45 GHz frequency for the industrial, scientific, and medical (ISM) radio band applications. The proposed antenna consisted of bisectional dipole core, a pair of quarter-wave baluns, and four diagonally adjoined parasitic braces. The bisectional dipole core was utilized to improve the antenna gain and realize omnidirectional radiation pattern, and the quarter-wave baluns were to symmetrize the current on the bisectional core. The four parasitic braces collectively generated circular polarization. In the study, simulations were conducted using CST Microwave Studio and a prototype antenna fabricated. To validate, experiments were carried out, and simulation and experimental results compared. The finding revealed good agreement between the simulation and experimental results. Essentially, in addition to achieving an antenna gain of 2.07 dBic, the proposed CP single-fed omnidirectional antenna is suited to ISM frequency band applications.

1. Introduction

In modern wireless communication, transmitting and receiving antennas with omnidirectional radiation pattern are preferable. Nevertheless, omnidirectionality gives rise to multipath wave reflections and phase error in the receiving antenna. As a result, circular polarization is adopted to rectify the multipath effect.

In theory, circular polarization of a patch antenna is realized by exciting two orthogonal components of identical amplitude [1]. Specifically, in [2], a circular monopolar patch antenna with U-slot patch and four slots achieved dual-band (2.45 and 5.8 GHz) CP omnidirectional radiation pattern at the respective gains of 1.37 and 4.37 dBi. In [3], a CP quad-band antenna using metamaterial was proposed. In [4], an antenna with four bended monopoles excited by feeding network was used to realize circular polarization with impedance bandwidth of 3.56% at 2.44 GHz and an average gain of 1.39 dBi. In [5], bended dipoles integrated with baluns were used to realize circular polarization with 2.32-2.61 GHz axial ratio bandwidth and a gain of 1.2 dBic. In [6], a circular slot fed by an L-shaped strip was proposed to realize circular polarization. The antenna gains in [2–6] were less than satisfactory, however.

In [7], a quarter-wave shorted patch connected with two-PCB strip was utilized to generate circular polarization with impedance bandwidth of 4.3% at 5.8 GHz. In [8], a weak-coupling mechanism was incorporated into feeding network to realize high gain and wide 3-dB AR bandwidth. In [9], a 2.4 GHz two-faced slot CP antenna was proposed to realize

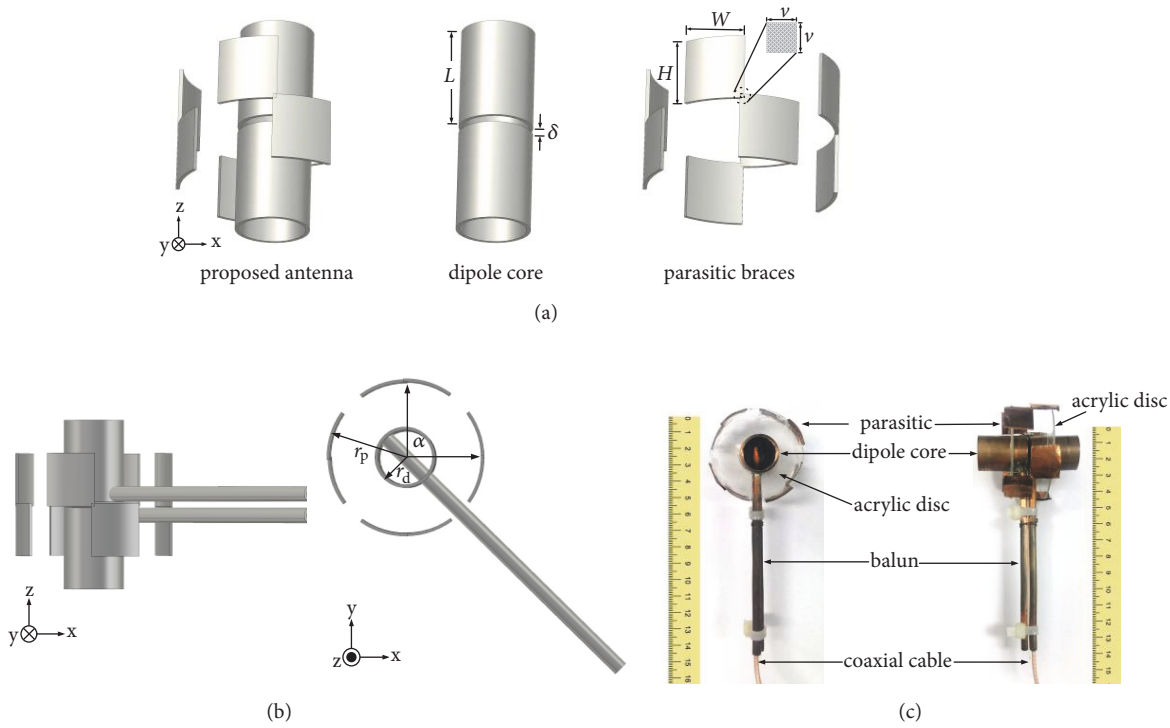

Figure 1: The circularly polarized single-fed omnidirectional dipole antenna: (a) geometry, (b) configuration with balun, (c) prototype.

circular polarization. In [10], two off-center-fed dipoles were proposed to realize a broadband CP antenna.

In [11], a CP antenna with rotatable dipole-shaped radiation pattern achieved impedance bandwidth of 2.4-2.51 GHz with a gain of 1.9 dBic. In [12], circular polarization was realized using a circular patch with six vortex slots and six shorting pins. In [13], four arcs were incorporated to improve circular polarization of a patch antenna. In [14], elliptical-ring slot was deployed surrounding the main patch to improve circular polarization. In [15], a circular patch connected to ground plane by conductive vias achieved wideband CP but low antenna gain. The antennas in [11–15] required multilayered PCB and shorting vias.

In [16], a dielectric resonator antenna (DRA) achieved CP omnidirectional radiation pattern. In [17], a rectangular DRA above the ground plane could achieve dual frequency of 1.58 GHz and 2.4 GHz. In [18], four 30°-rotated rectangular dielectric layers generated 90°-phase current difference between layers, thus achieving circular polarization. In [19], a DRA could achieve CP radiation pattern with impedance matching of -40 dB. In [20], a 2.4 GHz CP antenna with top-loaded Alford loop was proposed. In [21], a CP DRA fed by microstrip line achieved a 3-dB AR bandwidth of 85 MHz at 2.45 GHz frequency. However, the dielectric resonator antennas in [16–21] suffered from fabrication complexity.

In [22–24], omnidirectional dipole antennas could achieve improved impedance bandwidth and high antenna gains. However, they failed to realize circular polarization. In [25], a CP array antenna with parallel striplines achieved 3-dB AR between 890 and 930 MHz with omnidirectional radiation pattern. In [26], a feeding probe and parasitic dielectric paralleled pipe element achieved a 3-dB AR bandwidth of 54.9% with omnidirectional radiation pattern. In [27], a torus-knot antenna could achieve CP omnidirectional beam. In [28], an antenna using two orthogonally aligned circles achieved a 3-dB AR bandwidth of 58% with omnidirectional radiation pattern.

Specifically, the aim of this research is to propose a circularly polarized single-fed omnidirectional dipole antenna operable in 2.45 GHz center frequency for ISM band applications. The proposed CP omnidirectional antenna was comprised of bisectional dipole core, a pair of quarter-wave baluns, and four diagonally adjoined parasitic braces. The bisectional core (upper and lower core sections) was deployed to enhance the antenna gain and realize omnidirectional radiation pattern, while the baluns symmetrized the current on the upper and lower core sections. Circular polarization was realized by four diagonally adjoined parasitic braces. Simulations were performed using CST Microwave Studio [29] and an antenna prototype fabricated. Experiments were subsequently carried out and simulation and experimental results compared, including matching impedance, the 3-dB axial ratio bandwidth, gain, and 3-dB axial ratio beamwidth.

2. Antenna Structure

Figures 1(a) and 1(b) illustrate the geometry of the circularly polarized (CP) single-fed omnidirectional dipole antenna, consisting of bisectional dipole core, a pair of quarter-wave baluns, and four diagonally adjoined parasitic braces. The CP omnidirectional antenna was 52×52×56 mm in size. The copper dipole core was of two sections: upper and lower

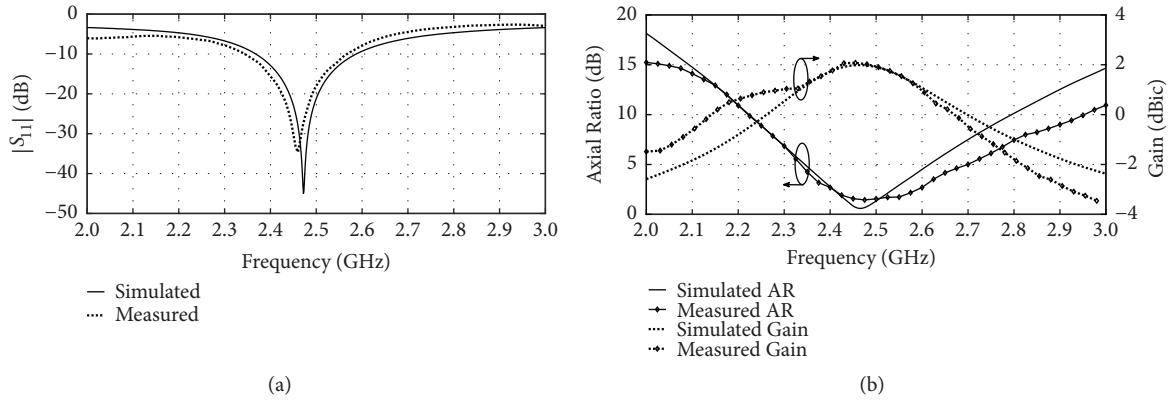

Figure 2: Simulation and measured results of the CP single-fed omnidirectional dipole antenna: (a) $|S_{11}|$, (b) AR and gain.

sections, whose distance (δ) was 2 mm. The radius (r_d) and thickness of the dipole core were 10 and 1 mm. The length of each core section (L) was 27 mm and perpendicular to the quarter-wave baluns. The bisectional core was connected to a coaxial feed via balun. The bisectional dipole core was utilized to obtain omnidirectional radiation pattern. Meanwhile, the parasitic braces were incorporated to generate circular polarization.

Each parasitic brace resembled two diagonally adjoined rectangular copper plates of identical size, with 17.5, 16, and 1 mm in height (H), width (W), and thickness. The adjoining region between both rectangular plates (v^2) was 1 mm^2. There were four diagonally adjoined parasitic braces enclosing the bisectional core. The void space between the parasitic braces and core center was 26 mm in distance or $\lambda/5$ where λ is the wavelength at the center frequency (2.45 GHz). The parasitic braces were individually placed at an angle (α) of 90° in relation to adjacent braces to generate circular polarization. Interestingly, the thickness of parasitic braces beyond 1 mm shifted the resonant frequency of impedance matching ($|S_{11}|$) and axial ratio (AR) to lower frequencies, thereby worsening $|S_{11}|$.

Figure 1(b) depicts the two copper quarter-wave baluns placed in parallel (2 mm apart) and individually connected to the bisectional core. The balun was 100, 5, and 1 mm in length, diameter, and thickness. The baluns were then shorted at a distance of 30 mm from the dipole core. The pair of baluns were utilized to induce current symmetry on the bisectional core.

Figure 1(c) shows a prototype of the 2.45 GHz CP single-fed omnidirectional dipole antenna. The bisectional dipole core individually connected to the two copper baluns. The 50-Ω SMA-type coaxial cable was used to feed the signal. The core and ground structure of the coaxial cable were individually connected to the bisectional dipole core through the balun. Two acrylic discs individually attached to the upper and lower sections of the dipole core. The parasitic braces adhered to both of the acrylic discs along their curves and made the bisectional core apart. Table 1 tabulates the optimal parameters of the proposed CP single-fed omnidirectional antenna operable at 2.45 GHz center frequency.

3. Simulation and Measurement Results

The antenna prototype was then experimented and results were compared with simulation results. Figure 2(a) compares the simulation and measured $|S_{11}|$. The simulation and measured $|S_{11}|$ (<-10 dB) covered 2.37-2.59 GHz (8.87%) and 2.35-2.57 GHz (8.94%), respectively, encompassing the ISM frequency band of 2.4-2.484 GHz. In Figure 2(b), the simulation and measured realized gains over the ISM band were 1.98 and 2.07 dBic. Meanwhile, the simulation and measured 3-dB AR bandwidth at the center frequency were 2.40-2.55 GHz (6.06%) and 2.40-2.60 GHz (8.00%).

Figures 3(a) and 3(b), respectively, illustrate the simulation and measured AR in the x-z and y-z planes at 2.45 GHz. The simulation and measured AR of both x-z and y-z planes were symmetrical and of right-hand circular polarization (RHCP). In Figure 3(a), the simulation and measured axial ratio beamwidth (AR-BW) in the x-z plane were 54° and 65°, respectively. The corresponding AR-beamwidths in the y-z plane were identical (i.e., 360°).

Figures 4(a) and 4(b), respectively, illustrate the simulation and measured radiation patterns in the x-z and y-z planes at 2.45 GHz. The radiation patterns were symmetrical and omnidirectional with RHCP. In the x-z plane, the simulation and measured AR-beamwidth were 74° and 75°, respectively, and the corresponding AR-beamwidths in the y-z plane were also identical (360°).

Table 2 compares the simulated and measured $|S_{11}|$, AR, half-power beamwidth, AR-BW, gain, and polarization at 2.45 GHz operating frequency. The simulation and experimental results exhibited good agreement.

4. Design, Parametric Study, and Analysis

4.1. Evolutionary Stages of Proposed Antenna. Figure 5 illustrates the four evolutionary stages of the antenna, including conventional 6mm-Ø dipole core without parasitic brace (scheme A), with single parasitic brace (scheme B) and four parasitic braces (scheme C), and expanded 20mm-Ø dipole core with four parasitic braces (scheme D). Figures 6(a) and 6(b), respectively, illustrate the simulated $|S_{11}|$ and AR under

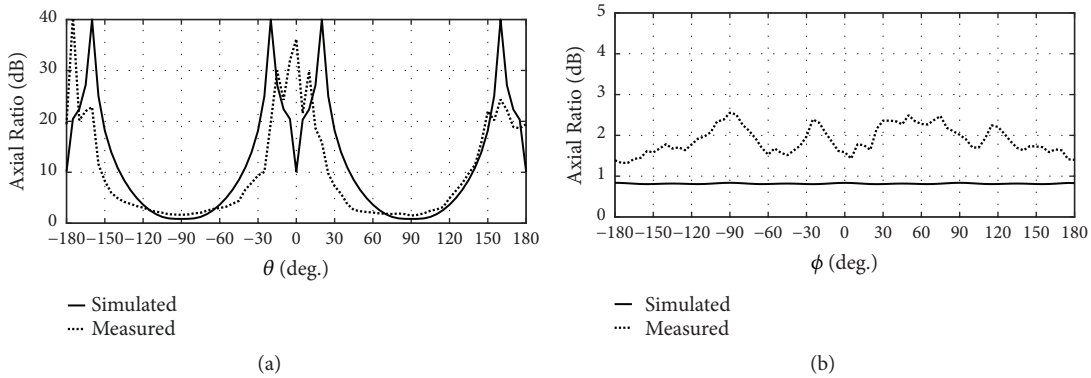

Figure 3: Simulation and measured AR of the CP single-fed omnidirectional dipole antenna at 2.45 GHz: (a) *x-z*, (b) *y-z* plane.

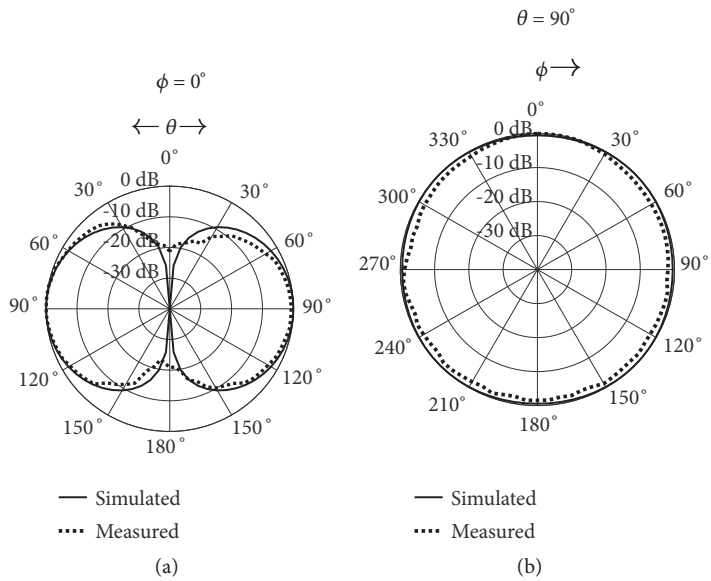

Figure 4: Simulation and measured radiation patterns of the CP single-fed omnidirectional dipole antenna at 2.45 GHz: (a) *x-z*, (b) *y-z* plane.

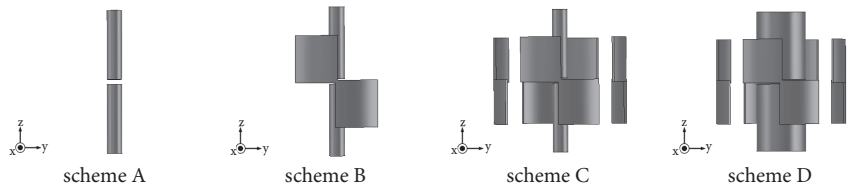

Figure 5: The evolutionary stages of CP single-fed omnidirectional antenna.

Table 1: Parameters of the CP omnidirectional dipole antenna operable at 2.45 GHz.

Parameter	Description	Electrical size	Physical size
L	Length of sectional core (single section)	0.22λ	27.0 mm
δ	Distance between bi-sectional cores	0.02λ	2.0 mm
r_d	Radius of bi-sectional core	0.08λ	10.0 mm
W	Width of rectangular plate	0.13λ	16.0 mm
H	Height of rectangular plate	0.14λ	17.5 mm
v	Adjoining region of two rectangular plates	0.01λ	1.0 mm
r_p	Distance between parasitic braces and core center	0.21λ	26.0 mm
α	Angle between two adjacent plates	90.0°	

Table 2: Characteristics of CP single-fed omnidirectional antenna operable at 2.45 GHz.

Characteristics	Simulation	Measured
$\|S_{11}\|$	2.37 – 2.59 GHz	2.35 – 2.57 GHz
AR	2.40 – 2.55 GHz	2.40 – 2.60 GHz
HPBW		
x–z	74°	75°
y–z	360°	360°
3-dB AR-BW		
x–z	54°	65°
y–z	360°	360°
Gain	1.98 dBic	2.07 dBic
Polarization	RHCP	RHCP

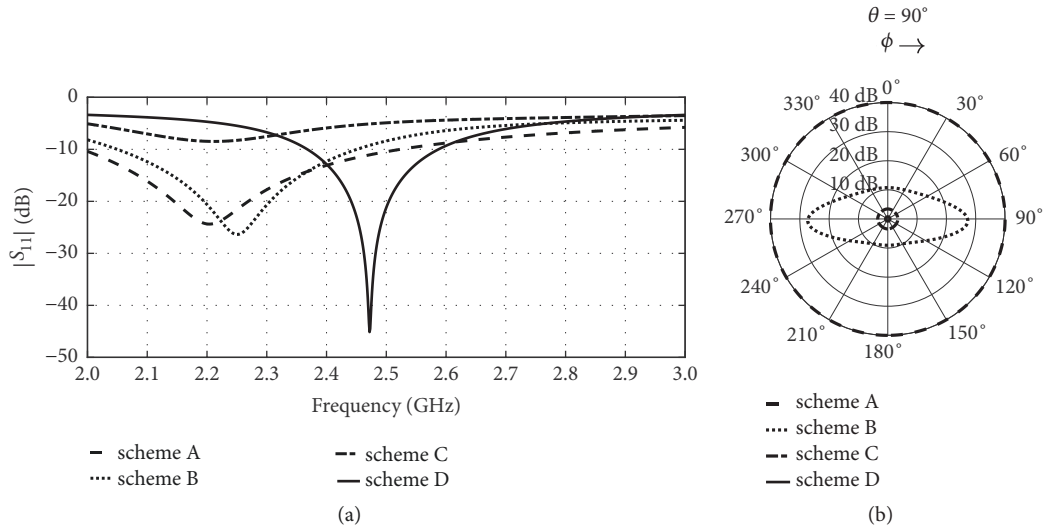

Figure 6: The evolutionary stages of CP single-fed omnidirectional antenna: (a) simulated $|S_{11}|$, (b) AR.

scheme A, scheme B, scheme C, and scheme D using CST Microwave Studio.

In schemes A and B, the simulated $|S_{11}|$ was below -10 dB ($|S_{11}|$ < -10 dB), but both schemes failed to achieve circular polarization (AR = 40 dB and 27 dB for schemes A and B). In scheme C, the antenna failed to achieve impedance matching ($|S_{11}|$ > -10 dB) despite AR approaching 3.0 dB. Meanwhile, scheme D achieved $|S_{11}|$ and circular polarization (AR<3.0 dB) at the 2.45 GHz center frequency. The optimal radius of the dipole core (r_d) with four parasitic braces was thus 10 mm.

4.2. Length of One Single Section of the Dipole Core (L). Figures 7(a)–7(c), respectively, illustrate the simulated $|S_{11}|$, AR, gain, and half power beamwidth (HPBW) under variable lengths of dipole core (single section): 21, 24, 27, 30, and 33 mm. The findings revealed that, with increase in L, the resonant frequency of $|S_{11}|$ became lower while that of AR became minimally higher. The effects were expected because it is well known that resonant frequency decreases with an increase in the length of dipole core. The optimal L was 27 mm, where $|S_{11}|$ < -10 dB and AR < 3 dB at 2.45 GHz frequency. In Figure 7(c), the maximum gain was in the vicinity of the 2dBic standard dipole, given L between 27 and 30 mm, which is the vicinity of half-wave dipole core. Meanwhile, the HPBW of x-z plane decreased with increase in the length of dipole core. The HPBW of the optimal L (27 mm) was thus 74 degrees.

4.3. Distance between Upper and Lower Core Sections (δ). Figures 8(a)–8(c), respectively, illustrate the simulated $|S_{11}|$, AR, gain, and HPBW under variable distances between two sections of the dipole core (δ): 1.0, 1.5, 2.0, 2.5, and 3.0 mm. The findings showed that δ below or above 2.0 mm resulted in the resonant frequency of $|S_{11}|$ falling outside the target operating frequency (2.45 GHz), while variation in δ had negligible impact on AR. Since δ had no effect on AR, it could be used to tune the resonant frequency of $|S_{11}|$ without the worry about the 3-dB AR. The optimal δ was thus 2 mm. In Figure 8(c), with δ below or above 2.0 mm, the gain became lower while variation in δ had negligible impact on HPBW because the length of dipole core was not changed.

4.4. Radius of Bisectional Dipole Core (r_d). Figures 9(a)–9(c), respectively, depict the simulated $|S_{11}|$, AR, gain, and HPBW under variable radii of bisectional dipole core (r_d): 3.0, 6.5, 10.0, 13.5, and 17.0 mm. In Figure 9(a), r_d below or above 10.0

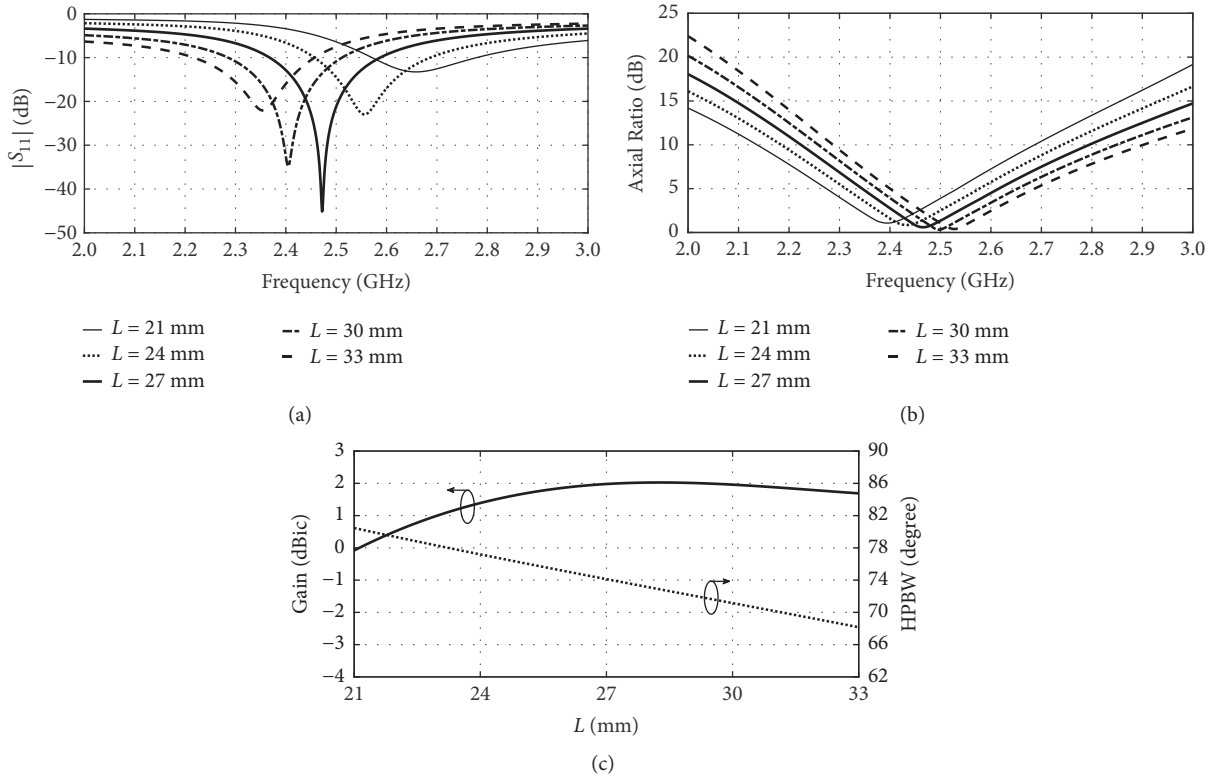

Figure 7: Simulation results under variable lengths (L) of dipole core (single section): (a) $|S_{11}|$, (b) AR, (c) gain and HPBW.

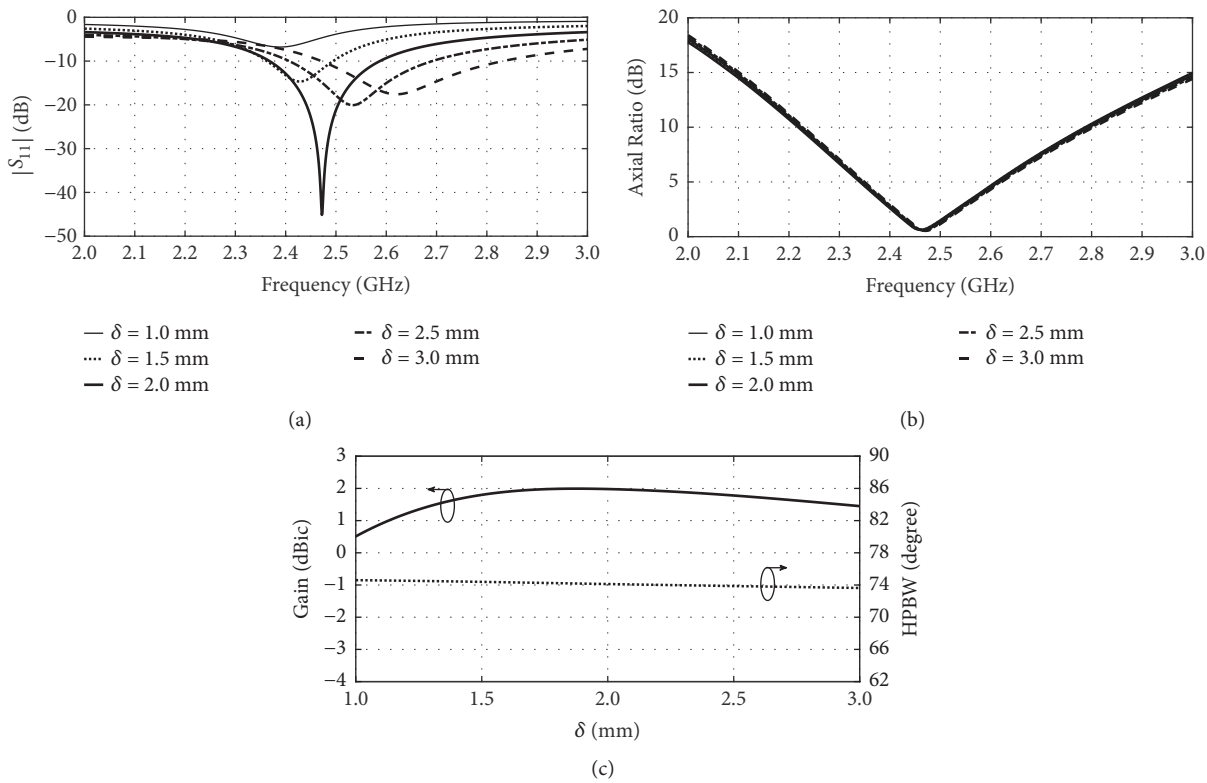

Figure 8: Simulation results under variable distances between two core sections (δ): (a) $|S_{11}|$, (b) AR, (c) gain and HPBW.

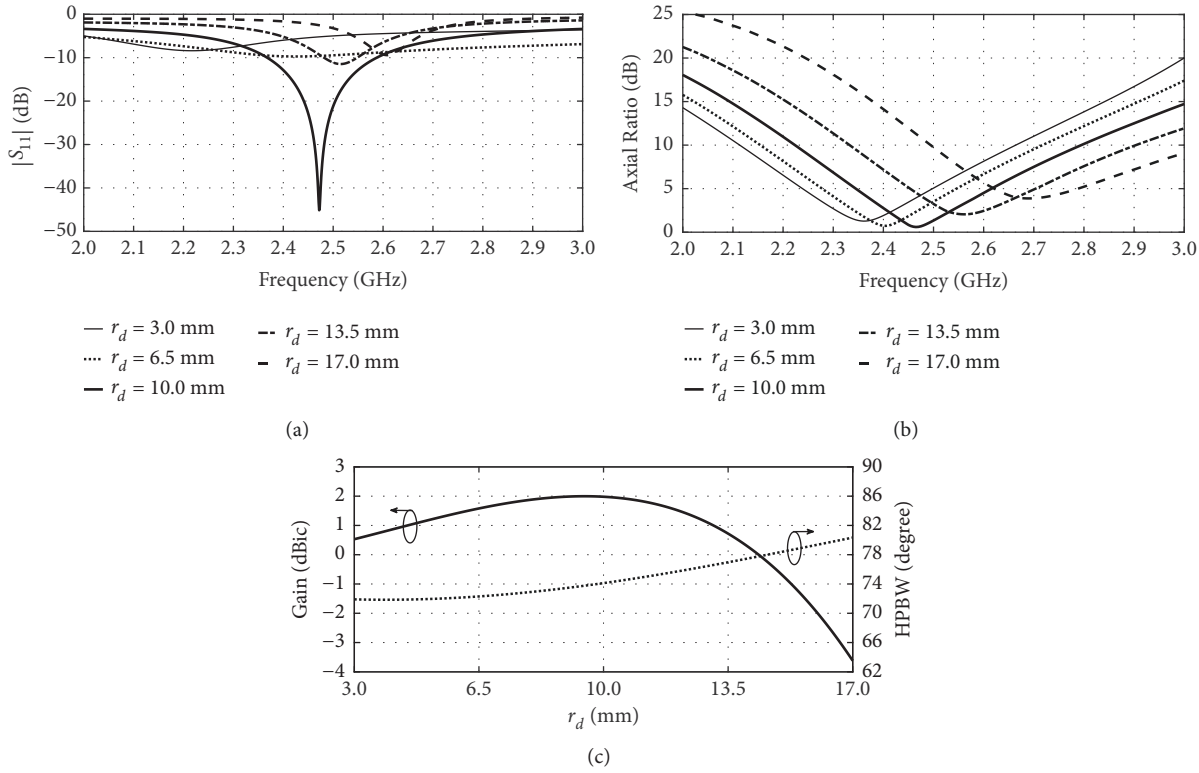

Figure 9: Simulation results under variable radii of the dipole core (r_d): (a) $|S_{11}|$, (b) AR, (c) gain and HPBW.

mm gave rise to the resonant frequency of $|S_{11}|$ falling outside the center frequency (2.45 GHz). Meanwhile, the resonant frequency of AR increased with increase in the core radius. The $|S_{11}|$ and AR resonant frequencies were sensitive to r_d. The optimal r_d was thus 10.0 mm. In Figure 9(c), r_d below or above 10.0 mm gave worse to the gain. Meanwhile, the HPBW increased with increase in the core radius.

4.5. Width of Rectangular Parasitic Plate (W). Figures 10(a)–10(c), respectively, illustrate the simulated $|S_{11}|$, AR, gain, and HPBW under variable rectangular parasitic plate widths (W): 13.0, 14.5, 16.0, 17.5, and 19.0 mm. As previously discussed, four diagonally adjoined parasitic braces were deployed to realize circular polarization at the 2.45 GHz center frequency. The simulation results indicated that the resonant frequency of $|S_{11}|$ and AR approached the center frequency (2.45 GHz) as W increased. However, W beyond 16.0 mm adversely affected $|S_{11}|$ and AR resonant frequencies because they directly affected the field coupling between the bisectional dipole core and the parasitic plates. It was found that resonant frequency decreases with an increase in the width of rectangular parasitic plate. The optimal W was thus 16.0 mm. In Figure 10(c), W below or above 16.0 mm gave worse to the gain. The HPBW increased with increase in the width of rectangular parasitic plate between 14.5 and 17.5 mm.

4.6. Length of Rectangular Parasitic Plate (H). Figures 11(a)–11(c), respectively, show the simulated $|S_{11}|$, AR, gain, and HPBW under variable rectangular parasitic plate lengths (H): 11.5, 14.5, 17.5, 20.5, and 23.5 mm. The findings revealed that the resonant frequency of $|S_{11}|$ and AR approached the target frequency (2.45 GHz) as H increased. Nonetheless, H beyond 17.5 mm shifted $|S_{11}|$ and AR resonant frequencies below the target frequency. It was found that the effects were similar to those of W. The optimal H was thus 17.5 mm. In Figure 11(c), H below or above 17.5 mm gave worse to the gain. The HPBW increased with increase in the length of rectangular parasitic plate between 17.5 and 23.5 mm, while variation in H between 11.5 and 17.5 mm had negligible impact on HPBW.

4.7. Distance between Parasitic Brace and the Core Center (r_p). Figures 12(a)–12(c), respectively, illustrate the simulated $|S_{11}|$, AR, gain, and HPBW under variable distances between parasitic brace and the core center (r_p): 22, 24, 26, 28, and 30 mm. The simulation results showed that the resonant frequency of $|S_{11}|$ approached the target center frequency (2.45 GHz) as r_p increased. However, beyond the 26mm threshold, the $|S_{11}|$ resonant frequency was below the target frequency. The AR resonant frequency was in the vicinity of the target frequency, given r_p between 24 and 30 mm. The resonant frequency of AR was below the target frequency for r_p of 22 mm. The adjustment of r_p was less affected than the adjustment of r_d. The optimal r_p was 26 mm. The variation in r_p had negligible impact on the gain. Meanwhile, the HPBW decreased with increase in the distance between parasitic brace and the core center.

4.8. Current Vector Distribution on Diagonally Adjoined Parasitic Brace. Figure 13 illustrates the simulated current vector

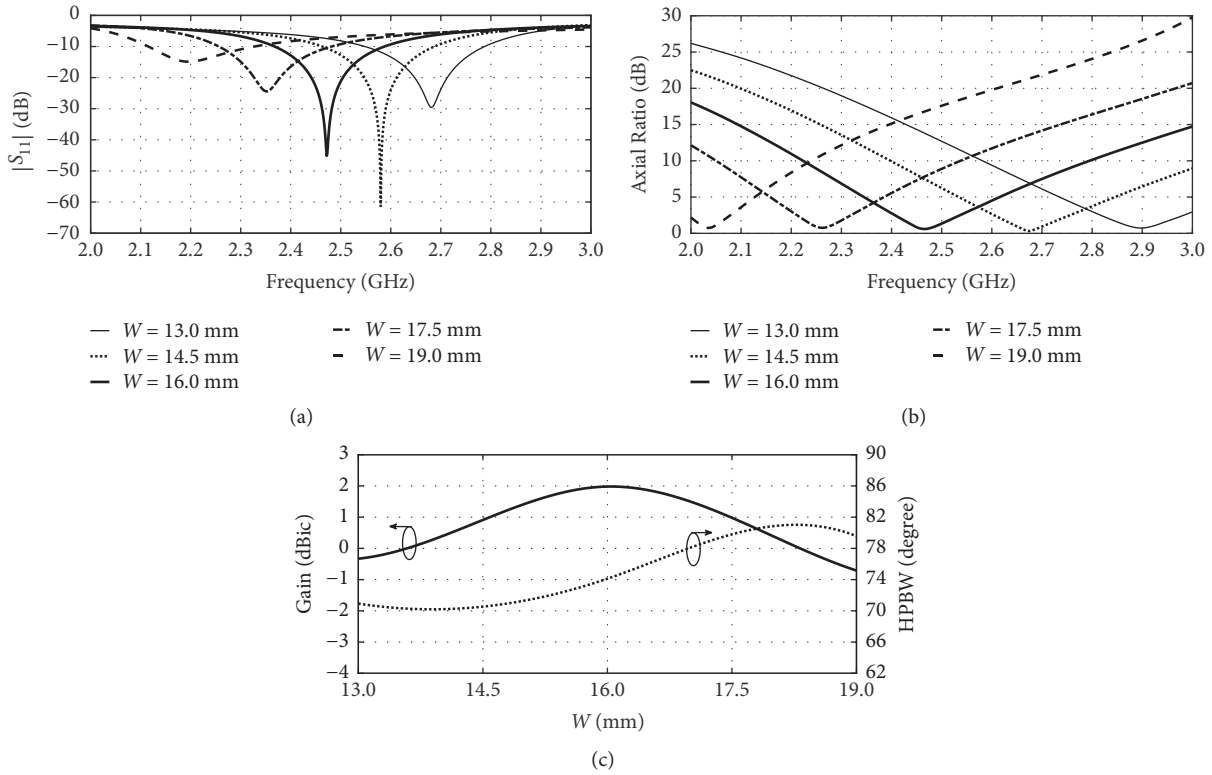

Figure 10: Simulation results under variable rectangular plate widths (W): (a) $|S_{11}|$, (b) AR, (c) gain and HPBW.

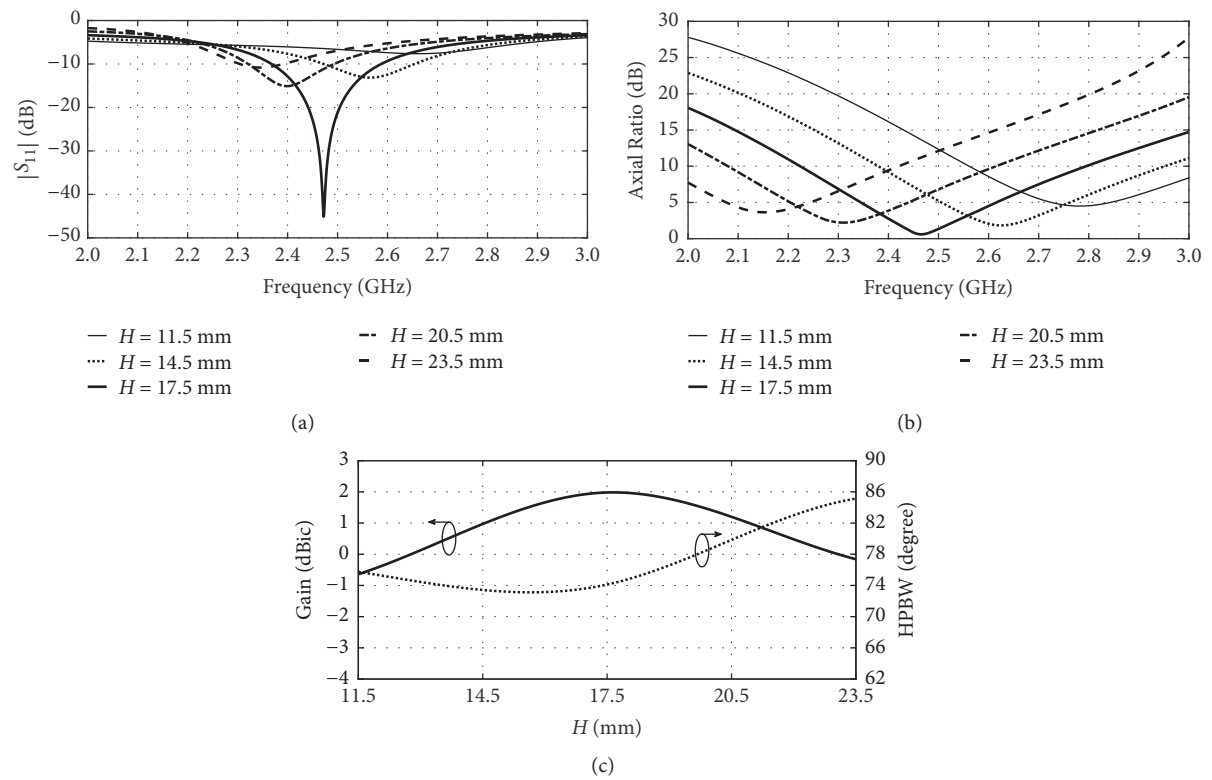

Figure 11: Simulation results under variable rectangular plate lengths (H): (a) $|S_{11}|$, (b) AR, (c) gain and HPBW.

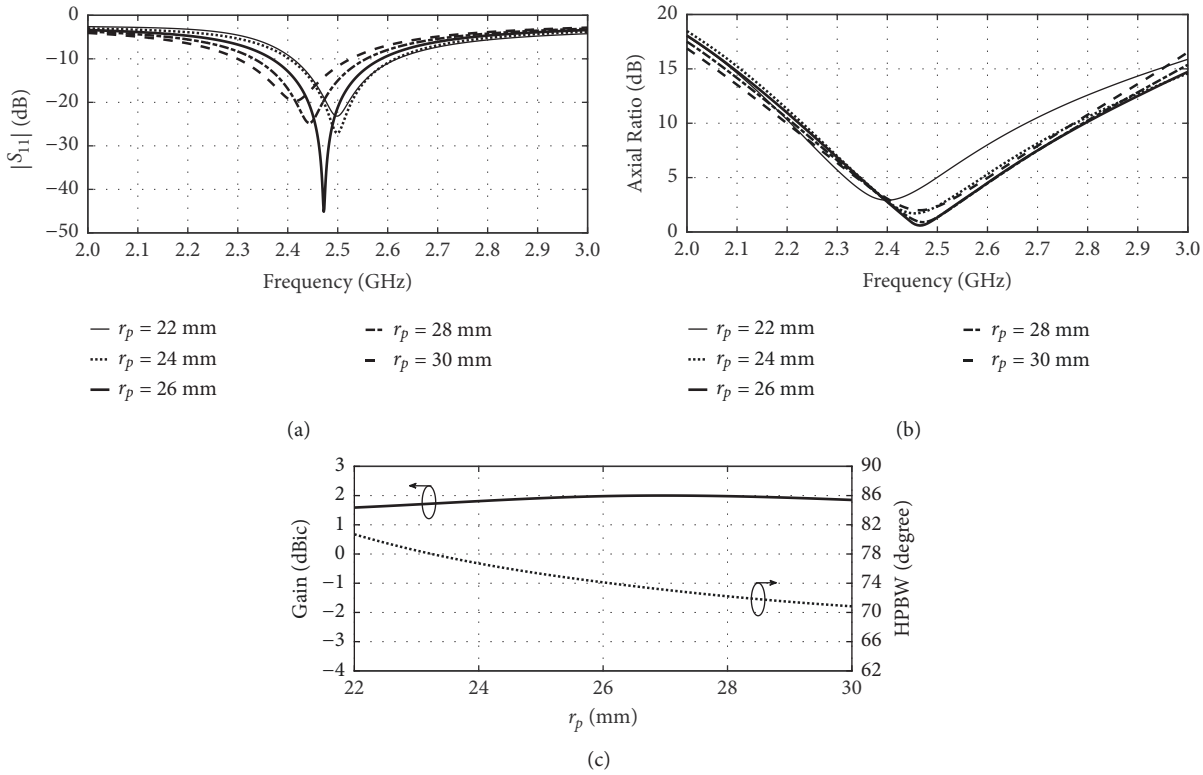

Figure 12: Simulation results under variable distances between parasitic brace and the core center (r_p): (a) $|S_{11}|$, (b) AR, (c) gain and HPBW.

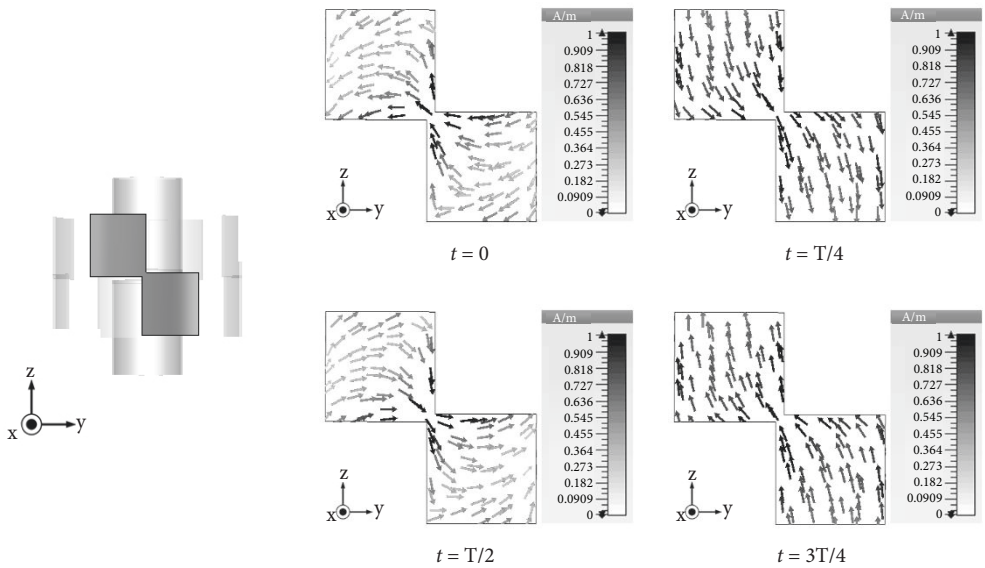

Figure 13: Current vector distribution on a single diagonally adjoined parasitic brace.

distribution on a single diagonally adjoined parasitic brace relative to time (t). The magnitude of current vector was identical with 90° phase difference, independent of time. At 2.45 GHz, the direction of surface current was counterclockwise as time (t) shifted from 0, T/2, T/4, to 3T/4. The collective use of four diagonally adjoined parasitic braces thus generated circular polarization.

5. Comparison between CP Omnidirectional Antennas

The overall dimension of the proposed antenna is 52 mm × 52 mm × 56 mm, excluding the baluns and the coaxial connector. The baluns are necessary to symmetrize the current on the bisectional core and shorted at a distance

Table 3: Comparison between CP omnidirectional antennas.

Ref.	Impedance bandwidth	AR bandwidth	Gain	Size (mm^3)	Radiation Pattern
5	2.32 – 2.54 GHz	2.32 – 2.61 GHz	1.20 dBic	33 × 33 × 20	Omnidirectional
11	2.40 – 2.51 GHz	2.46 – 2.48 GHz	1.90 dBic	80 × 46 × 6	Omnidirectional
15	2.27 – 2.77 GHz	2.25 – 2.73 GHz	3.75 dBic	180 × 180 × 3	Omnidirectional
16	2.30 – 2.94 GHz	2.39 – 2.57 GHz	0.91 dBic	39 × 39 × 33	Omnidirectional
19	2.37 – 2.63 GHz	2.37 – 2.56 GHz	1.56 dBic	53 × 53 × 20	Omnidirectional
20	2.39 – 2.51 GHz	2.39 – 2.51 GHz	1.12 dBic	50 × 50 × 20	Omnidirectional
proposed	2.35 – 2.57 GHz	2.40 – 2.60 GHz	2.07 dBic	52 × 52 × 56	Omnidirectional

of 30 mm from the bisectional core. The long baluns are used to support the measurement setup. For comparison of the various performance, some antennas in the references are not radiating CP with the omnidirectional radiation pattern, and some antennas operate outside 2.4-2.484 GHz. Thus, the related CP omnidirectional antennas encompassing the ISM frequency band of 2.4-2.484 GHz are listed in Table 3. In the comparison, the antennas in [5, 16] are smaller than the proposed antenna, but it achieved a low gain. Moreover, the feeding network was required in [5]. The antenna in [11] achieved a similar gain to the proposed antenna, but it suffered from bulkiness. The antenna in [15] has the highest gain, but its size is the biggest (more than 3 times compared with the proposed antenna). Meanwhile, the antenna in [19, 20] achieved a similar size to the proposed antenna, but their gains were lower, and they used multiport feeding. For antennas operating in 2.4-2.484 GHz band, the proposed antenna possesses compromised performance because it has the high gain with the compact size. The advantages of the proposed antenna are that they possessed a similar gain to the standard dipole antenna, a single-fed antenna, and no feeding network was required in the antenna structure.

6. Conclusion

This research proposed a 2.45 GHz circularly polarized single-fed omnidirectional dipole antenna for ISM frequency band applications. The CP omnidirectional antenna consisted of bisectional dipole core (upper and lower sections), a pair of quarter-wave baluns, and four diagonally adjoined parasitic braces. The bisectional dipole core was utilized to enhance the antenna gain and realize omnidirectional radiation pattern, and the quarter-wave baluns were to symmetrize the current on the upper and lower core sections. The four parasitic braces were incorporated to induce circular polarization. The measured $|S_{11}|$ bandwidth, 3-dB AR bandwidth, gain, and 3-dB AR beamwidth in x-z plane were 2.35-2.57 GHz (8.94%), 2.40-2.60 GHz (8.00%), 2.07 dBic, and 65°. In essence, the proposed CP omnidirectional antenna could achieve a high antenna gain and is suited to ISM frequency band applications.

Data Availability

The data used to support the findings of this study are available from the corresponding author upon request.

Conflicts of Interest

The authors declare that there is no conflict of interests regarding the publication of this paper.

Acknowledgments

This research was funded by the College of Industrial Technology, King Mongkut's University of Technology North Bangkok (Grant No. RES-CIT0321/2018). This work has also been supported by the Thailand Research Fund through the TRF Senior Research Scholar Program with Grant No. RTA6080008.

References

[1] C. A. Balanis, *Antenna Theory: Analysis and Design*, Wiley, New York, NY, USA, 1997.

[2] X.-Q. Zhu, Y.-X. Guo, and W. Wu, "A novel dual-band antenna for wireless communication application," *IEEE Antennas and Wireless Propagation Letters*, vol. 15, pp. 516–519, 2016.

[3] M. Venkateswara Rao, B. T. P. Madhav, T. Anilkumar, and B. Prudhvi Nadh, "Metamaterial inspired quad band circularly polarized antenna for WLAN/ISM/Bluetooth/WiMAX and satellite communication applications," *AEU - International Journal of Electronics and Communications*, vol. 97, pp. 229–241, 2018.

[4] Y. Yu, Z. Shen, and S. He, "Compact omnidirectional antenna of circular polarization," *IEEE Antennas and Wireless Propagation Letters*, vol. 11, pp. 1466–1469, 2012.

[5] Y. Yu, J. Xiong, and H. Li, "Compact omni-directional circularly polarised antenna utilising bended dipoles and integrated baluns," *IET Microwaves, Antennas & Propagation*, vol. 11, no. 10, pp. 1409–1414, 2017.

[6] C.-Y. Sim, "Conical beam array antenna with polarization diversity," *IEEE Transactions on Antennas and Propagation*, vol. 60, no. 10, pp. 4568–4572, 2012.

[7] J. Liu, Y. Li, Z. Liang, and Y. Long, "A planar quasi-magnetic-electric circularly polarized antenna," *IEEE Transactions on Antennas and Propagation*, vol. 64, no. 6, pp. 2108–2114, 2016.

[8] Q. Liu, Z. N. Chen, Y. Liu, and C. Li, "Compact ultrawideband circularly polarized weakly coupled patch array antenna," *IEEE Transactions on Antennas and Propagation*, vol. 65, no. 4, pp. 2129–2134, 2017.

[9] J. Wu and K. Sarabandi, "Compact omnidirectional circularly polarized antenna," *IEEE Transactions on Antennas and Propagation*, vol. 65, no. 4, pp. 1550–1557, 2017.

[10] R. Li, L. Pan, and Y. Cui, "A novel broadband circularly polarized antenna based on off-center-fed dipoles," *IEEE Transactions on Antennas and Propagation*, vol. 63, no. 12, pp. 5296–5304, 2015.

[11] A. Narbudowicz, X. Bao, M. Ammann, H. Shakhtour, and D. Heberling, "Circularly polarized antenna with steerable dipole-like radiation pattern," *IEEE Transactions on Antennas and Propagation*, vol. 62, no. 2, pp. 519–526, 2014.

[12] D. Yu, S.-X. Gong, Y.-T. Wan, Y.-L. Yao, Y.-X. Xu, and F.-W. Wang, "Wideband omnidirectional circularly polarized path antenna based on vortex slots and shorting vias," *IEEE Transactions on Antennas and Propagation*, vol. 62, no. 8, pp. 3970–3977, 2014.

[13] Y. Ma, J. Li, and R. Xu, "Design of an omnidirectional circularly polarized antenna," *IEEE Antennas and Wireless Propagation Letters*, vol. 16, pp. 226–229, 2017.

[14] D. Yu, S.-X. Gong, Y.-T. Wan, and W. Jiang, "Wideband conical-beam circularly polarized microstrip antenna for large ground plane," *IEEE Transactions on Antennas and Propagation*, vol. 63, no. 10, pp. 4614–4619, 2015.

[15] Y. M. Pan, S. Y. Zheng, and B. J. Hu, "Wideband and low-profile omnidirectional circularly polarized patch antenna," *IEEE Transactions on Antennas and Propagation*, vol. 62, no. 8, pp. 4347–4351, 2014.

[16] Y. M. Pan, K. W. Leung, and K. Lu, "Omnidirectional linearly and circularly polarized rectangular dielectric resonator antennas," *IEEE Transactions on Antennas and Propagation*, vol. 60, no. 2, pp. 751–759, 2012.

[17] X. Fang, K. W. Leung, and E. H. Lim, "Singly-fed dual-band circularly polarized dielectric resonator antenna," *IEEE Antennas and Wireless Propagation Letters*, vol. 13, pp. 995–998, 2014.

[18] S. Fakhte, H. Oraizi, and R. Karimian, "A novel low-cost circularly polarized rotated stacked dielectric resonator antenna," *IEEE Antennas and Wireless Propagation Letters*, vol. 13, pp. 722–725, 2014.

[19] W. Li, K. W. Leung, and N. Yang, "Omnidirectional dielectric resonator antenna with a planar feed for circular polarization diversity design," *IEEE Transactions on Antennas and Propagation*, vol. 66, no. 3, pp. 1189–1197, 2018.

[20] W. W. Li and K. W. Leung, "Omnidirectional circularly polarized dielectric resonator antenna with top-loaded alford loop for pattern diversity design," *IEEE Transactions on Antennas and Propagation*, vol. 61, no. 8, pp. 4246–4256, 2013.

[21] C.-C. Lin and J.-S. Sun, "Circularly polarized dielectric resonator antenna fed by off-centered microstrip line for 2.4-GHz ISM band applications," *IEEE Antennas and Wireless Propagation Letters*, vol. 14, pp. 947–949, 2015.

[22] Y. Luo and Z. N. Chen, "Compressed dipoles resonator at higher order modes with enhanced directivity," *IEEE Transactions on Antennas and Propagation*, vol. 65, no. 11, pp. 5697–5701, 2017.

[23] S. S. S. Nasser, W. Liu, and Z. N. Chen, "Wide bandwidth and enhanced gain of a low-profile dipole antenna achieved by integrated suspended metasurface," *IEEE Transactions on Antennas and Propagation*, vol. 66, no. 3, pp. 1540–1544, 2018.

[24] Y. Zhang, X. Y. Zhang, and Y.-M. Pan, "Low-profile planar filtering dipole antenna with omnidirectional radiation pattern," *IEEE Transactions on Antennas and Propagation*, vol. 66, no. 3, pp. 1124–1132, 2018.

[25] J. Shi, X. Wu, X. Qing, and Z. N. Chen, "An omnidirectional circularly polarized antenna array," *IEEE Transactions on Antennas and Propagation*, vol. 64, no. 2, pp. 574–581, 2016.

[26] Y.-M. Pan and K. W. Leung, "Wideband circularly polarized dielectric bird-nest antenna with conical radiation pattern," *IEEE Transactions on Antennas and Propagation*, vol. 61, no. 2, pp. 563–570, 2013.

[27] S. V. Kumar and A. R. Harish, "Generation of circularly polarized conical beam pattern using torus knot antenna," *IEEE Transactions on Antennas and Propagation*, vol. 65, no. 11, pp. 5740–5746, 2017.

[28] B. Yektakhah and K. Sarabandi, "A Wideband Circularly Polarized Omnidirectional Antenna Based on Excitation of Two Orthogonal Circular TE21 Modes," *IEEE Transactions on Antennas and Propagation*, vol. 65, no. 8, pp. 3877–3888, 2017.

[29] "CST microwave studio suite (user's manual)," 2006, [online] Available: https://www.cst.com/.